Distributing entanglement with separable states

Christian Peuntinger,[1,2,*] Vanessa Chille,[1,2,*] Ladislav Mišta, Jr.,[3] Natalia Korolkova,[4]
Michael Förtsch,[1,2] Jan Korger,[1,2] Christoph Marquardt,[1,2] and Gerd Leuchs[1,2]

[1]*Max Planck Institute for the Science of Light,*
Günther-Scharowsky-Str. 1 / Bldg. 24, Erlangen, Germany
[2]*Institute of Optics, Information and Photonics,*
University of Erlangen-Nuremberg, Staudtstraße 7/B2, Erlangen, Germany
[3]*Department of Optics, Palacký University,*
17. listopadu 12, 771 46 Olomouc, Czech Republic
[4]*School of Physics and Astronomy,*
University of St. Andrews, North Haugh,
St. Andrews, Fife, KY16 9SS, Scotland

(Dated: April 3, 2013)

*contributed equally to this work

Like a silver thread, quantum entanglement [1] runs through the foundations and breakthrough applications of quantum information theory. It cannot arise from local operations and classical communication (LOCC) and therefore represents a more intimate relationship among physical systems than we may encounter in the classical world. The 'nonlocal' character of entanglement manifests itself through a number of counterintuitive phenomena encompassing Einstein-Podolsky-Rosen paradox [2, 3], steering [4], Bell nonlocality [5] or negativity of entropy [6, 7]. Furthermore, it extends our abilities to process information. Here, entanglement is used as a resource which needs to be shared between several parties, eventually placed at remote locations. However entanglement is not the only manifestation of quantum correlations. Notably, also separable quantum states can be used as a shared resource for quantum communication. The experiment presented in this paper highlights the quantumness of correlations in separable mixed states and the role of classical information in quantum communication by demonstrating entanglement distribution using merely a separable ancilla mode.

The role of entanglement in quantum information is nowadays vividly demonstrated in a number of experiments. A pair of entangled quantum systems shared by two observers enables to teleport [8] quantum states between them with a fidelity beyond the boundary set by classical physics. Concatenated teleportations [9] can further span entanglement over large distances [10] which can be subsequently used for secure communication [11]. An a priori shared entanglement also allows to double the rate at which information can be sent through a quantum channel [12] or one can fuse bipartite entanglement into larger entangled cluster states being a 'hardware' for quantum computing [13].

The common feature of all entangling methods used so far is that entanglement is either produced by some global operation on the systems that are to be entangled or it results from a direct transmission of entanglement (possibly mediated by a third system) between the systems. Even entanglement swapping [9, 14], capable of establishing entanglement between the systems that do not have a common past, is not an exception to the rule because also here entanglement is directly transmitted between the participants.

However, quantum mechanics admits conceptually different means of establishing entanglement which are free of transmission of entanglement. Remarkably, creation of entangle-

ment between two observers can be disassembled into local operations and the communication of a *separable* quantum system between them [15]. The impossibility of entanglement creation by LOCC is not violated because communication of a quantum system is involved. The corresponding protocol exists only in a mixed-state scenario and obviously utilizes less quantum resources in comparison with the previous cases because communication of only a discordant [16–18] separable quantum system is required.

In this paper, we experimentally demonstrate the entanglement distribution by a separable ancilla [15] with Gaussian states of light modes [19]. The protocol aims at entangling mode A' which is in possession of a sender Alice with mode B' held by a distant receiver Bob by local operations and transmission of a separable mediating mode C' from Alice to Bob (see Fig. 1). This requires the parties to initiate their modes to a specific correlated but fully separable Gaussian state. Once the resource state $\hat{\rho}_{ABC}$ is established no further classical communication is needed to accomplish the protocol. To emphasize this, we attribute the state preparation process to a separate party, David. Note, that this resource state preparation is performed by LOCC only. No global quantum operation with respect to David's separated boxes is executed at the initial stage and no entanglement is present.

David's state $\hat{\rho}_{ABC}$ has to be equipped with the property that by a local operation on subsystem (AC) it can be transformed to a state $\hat{\rho}_{A'BC'}$ which is separable with respect to mode C', in order to guarantee that no entanglement is transmitted from Alice to Bob. It is also separable with respect to mode B', because no entanglement is a priori shared by Alice and Bob and the operation cannot create it. Mode A', however, has to be entangled with the composite subsystem (BC') so that the transmission of mode C' could establish entanglement between Alice and Bob. It means that despite the impossibility to entangle Alice with Bob by LOCC, we are requested to create entanglement of mode A' with a *delocalized* two-mode system (BC'), where mode C' belongs to Alice and mode B belongs to Bob by a local operation on Alice's part of the initial fully separable state. What is more, the entanglement of mode A' with two-mode system (BC') should be localizable between modes A' and B' by a local operation on Bob's side. The entanglement carried by the global state is in fact bound and the localization renders its activation [20] which de facto crowns the entanglement distribution.

The protocol

The task can indeed be accomplished in the three-step protocol [19] depicted in Fig. 1. We assign the preparation of the fully separable three-mode Gaussian resource state, with properties described above, to David. Initially modes A and C are prepared in a momentum squeezed and position squeezed vacuum state, respectively, with quadratures $\hat{x}_{A,C} = e^{\pm r}\hat{x}^{(0)}_{A,C}$, $\hat{p}_{A,C} = e^{\mp r}\hat{p}^{(0)}_{A,C}$, whereas mode B is in a vacuum state with quadratures $\hat{x}_B = \hat{x}^{(0)}_B$ and $\hat{p}_B = \hat{p}^{(0)}_B$. Here r is the squeezing parameter and the superscript "(0)" denotes the vacuum quadratures. David then exposes all the modes to suitably tailored local correlated displacements [21] (see also caption of Fig. 1):

$$\begin{aligned} \hat{p}_A &\rightarrow \hat{p}_A - p, \quad \hat{x}_C \rightarrow \hat{x}_C + x, \\ \hat{x}_B &\rightarrow \hat{x}_B + \sqrt{2}x, \quad \hat{p}_B \rightarrow \hat{p}_B + \sqrt{2}p, \end{aligned} \tag{1}$$

where the uncorrelated classical displacements x and p obey a zero mean Gaussian distribution with the same variance $(e^{2r} - 1)/2$. The state has been prepared by LOCC across $A|B|C$ splitting and hence is fully separable.

In the second step, modes A, C of the resource state are passed to Alice and mode B to Bob. Alice superimposes modes A and C on a balanced beam splitter BS_{AC}. The beam splitter cannot create entanglement with mode B and hence the state is separable with respect to $B|A'C'$ splitting. Moreover, the state also fulfills the positive partial transpose (PPT) criterion [22, 23] with respect to mode C' and hence it is also separable across $C'|A'B$ splitting [24] as required (see appendix).

In the final step, Alice sends mode C' to Bob who superimposes it with his mode B on another balanced beam splitter BS_{BC}. The presence of the entanglement between modes A' and B' can be certified by the sufficient criterion for entanglement by Duan *et al* [25], $T \equiv \langle(\hat{x}_{A'} - \hat{x}_{B'})^2\rangle + \langle(\hat{p}_{A'} + \hat{p}_{B'})^2\rangle < 2$. In the present case the total variance T reads as

$$T = \frac{1}{2} + \left(\frac{\sqrt{2}-1}{2}\right)^2 (2e^{2r} - 1) \; + \; \left(\frac{\sqrt{2}+1}{2}\right)^2 e^{-2r}$$

and it satisfies $T < 2$ if $r \leq \ln[(4 + 3\sqrt{2})/2] \doteq 1.42$. It clearly demonstrates the successful distribution of entanglement for a broad range of squeezing parameters r. This also confirms that mode A' was entangled with the two-mode system (BC') before the second beam

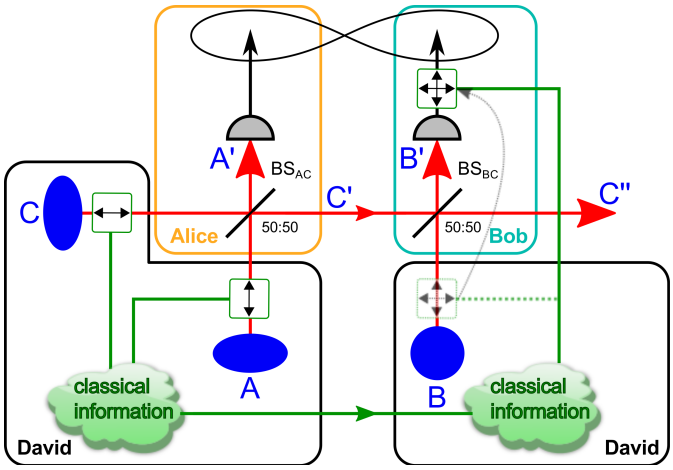

FIG. 1: **Sketch of the entanglement distribution protocol with continuous variables.** David prepares a momentum squeezed vacuum mode A, a position squeezed vacuum mode C and a vacuum mode B. He then applies random displacements (green boxes) of the $\hat{x}$ quadrature (horizontal arrow) and the $\hat{p}$ quadrature (vertical arrow) as in (1), which are correlated via classical communication channel (green line). David passes the modes A and C to Alice, and mode B to Bob. Alice superimposes the modes A and C on a balanced beam splitter BS_{AC} and communicates the separable mode C' to Bob. This is vital for the global entangling operation implemented by the protocol. Bob superimposes the received mode C' with his mode B on another balanced beam splitter BS_{BC}, which establishes entanglement between the output modes A' and B' (black lemniscata). Note the position of the displacement on mode B. In the original protocol the displacement is performed before BS_{BC}, which is depicted by the corresponding box with dashed green line. In this case, David provides Alice and Bob with a fully separable three-mode Gaussian resource state exhibiting the specific correlation properties described in the text. Sending of the separable ancilla mediates the generation of entanglement between the modes A' and B'. Equivalently, this displacement on mode B can be performed after BS_{BC} (dashed arrow indicates the respective relocation of displacement) on mode B', and even a posteriori on a measured mode B', as implemented in the experiment. The recovered entanglement is shown by the black lemniscata and confirmed by the experimental results. The solid red and green lines highlight the dual quantum-classical communication channel effectively present in the protocol: separable quantum communication (red) and the flow of classical information (green), respectively.

splitter, because otherwise the establishment of entanglement across $A'|B'$ splitting would not be possible.

In the experimental implementation, instead of quadratures we will work with polarization variables described by Stokes observables (see e.g. [26, 27]). We choose the state of polarization such that mean values of $\hat{S}_1$ and $\hat{S}_2$ equal zero while $\langle \hat{S}_3 \rangle \gg 0$. This configuration allows to identify the "dark" $\hat{S}_1$-$\hat{S}_2$-plane with the quadrature phase space. $\hat{S}_\theta, \hat{S}_{\theta+\pi/2}$ in this plane correspond to $\hat{S}_1, \hat{S}_2$ renormalized with respect to $\hat{S}_3 \approx S_3$ and can be associated with the effective quadratures $\hat{x}, \hat{p}$. We also use the modified version of the protocol indicated in Fig. 1 by the dashed arrow showing the alternative position of displacement in mode B: The random displacement applied by David can be performed after the beam splitter interaction of B and C', even a posteriori on the measured mode B'. This is technically more convenient and emphasizes that the classical information is sufficient for the entanglement recovery after the interaction of both modes A and B with the ancilla mode C and C', respectively.

Experiment

The experimental realization is divided in three steps, state preparation, measurement, and data processing, explained in detail in the methods section. David prepares two identically, polarization squeezed modes and adds noise in the form of random displacements to the squeezed observables. The Stokes observable $\hat{S}_\theta$ is identified with $\hat{p}$ and $\hat{S}_{\theta+\pi/2}$ with $\hat{x}$. These two Gaussian modes in a mixed state are provided to Alice and then interfered on the balanced beam splitter BS_{AC} with a relative phase of $\frac{\pi}{2}$ to ensure equal intensities of the output modes A' and C'.

The modulation patterns applied to modes A and C are chosen such that the two-mode state $\hat{\rho}_{A'C'}$ is separable. The states involved are Gaussian quantum states and, hence, are completely characterized by their first moments and the covariance matrix γ comprising all second moments (see appenix). The covariance matrix $\gamma_{A'C'}$ for this two-mode state has

been measured to be:

$$\gamma_{A'C'} = \begin{pmatrix} 20.90 \pm 0.0087 & 1.102 \pm 0.0091 & -7.796 \pm 0.0069 & -1.679 \pm 0.0076 \\ 1.102 \pm 0.0091 & 25.30 \pm 0.013 & 1.000 \pm 0.0071 & 14.63 \pm 0.0091 \\ -7.796 \pm 0.0069 & 1.000 \pm 0.0071 & 20.68 \pm 0.0093 & 0.8010 \pm 0.011 \\ -1.679 \pm 0.0076 & 14.63 \pm 0.0091 & 0.8010 \pm 0.011 & 24.65 \pm 0.0073 \end{pmatrix}. \quad (2)$$

A necessary and sufficient condition for separability of a Gaussian state $\hat{\rho}_{XY}$ of two modes X and Y with the covariance matrix γ_{XY} is given by the positive partial transpose (PPT) criterion [22, 23]:

$$\gamma_{XY}^{(T_Y)} + \mathrm{i}\Omega_2 \geq 0, \quad (3)$$

$$\Omega_2 = \bigoplus_{i=1}^{2} \begin{pmatrix} 0 & 1 \\ -1 & 0 \end{pmatrix}, \quad (4)$$

where $\gamma_{XY}^{(T_Y)}$ is the matrix corresponding to the partial transpose of the state $\hat{\rho}_{XY}$ with respect to the mode Y (see appendix). Effects that could possibly lead to some non-Gaussianity of the utilized states are discussed in detail also in the appendix. The state described by $\gamma_{A'C'}$ fulfils the condition (3) as the eigenvalues (39.84, 28.47, 13.85, 9.371) of $(\gamma_{A'C'}^{(T_{C'})} + \mathrm{i}\Omega_2)$ are positive, hence mode C' remains separable after BS_{AC}. Bob mixes the ancilla mode C' with a vacuum mode B on another balanced beam splitter, and performs a measurement on the transmitted mode B'. The measured two-mode covariance matrix of the output state $\gamma_{A'B'}$ is given by:

$$\gamma_{A'B'} = \begin{pmatrix} 19.95 \pm 0.011 & 1.025 \pm 0.016 & -4.758 \pm 0.0050 & -1.063 \pm 0.0051 \\ 1.025 \pm 0.016 & 22.92 \pm 0.012 & 0.9699 \pm 0.0047 & 9.153 \pm 0.0058 \\ -4.758 \pm 0.0050 & 0.9699 \pm 0.0047 & 9.925 \pm 0.0048 & 0.2881 \pm 0.0047 \\ -1.063 \pm 0.0051 & 9.153 \pm 0.0058 & 0.2881 \pm 0.0047 & 11.65 \pm 0.0038 \end{pmatrix}. \quad (5)$$

Again, the separability is proven by the PPT criterion (eigenvalues 28.24, 21.79, 8.646, 5.756). Only as Bob receives the classical information about the modulation on the initial modes A and C from David, he is able to recover the entanglement. After an appropriate post-processing of his measured raw data, Bob verifies that the Duan's criterion is violated [25]

$$\Delta^2_{\mathrm{norm}}(\hat{S}_{A',0^\circ} \cdot g + \hat{S}_{B',0^\circ}) \cdot \Delta^2_{\mathrm{norm}}(\hat{S}_{A',90^\circ} \cdot g - \hat{S}_{B',90^\circ}) < 1. \quad (6)$$

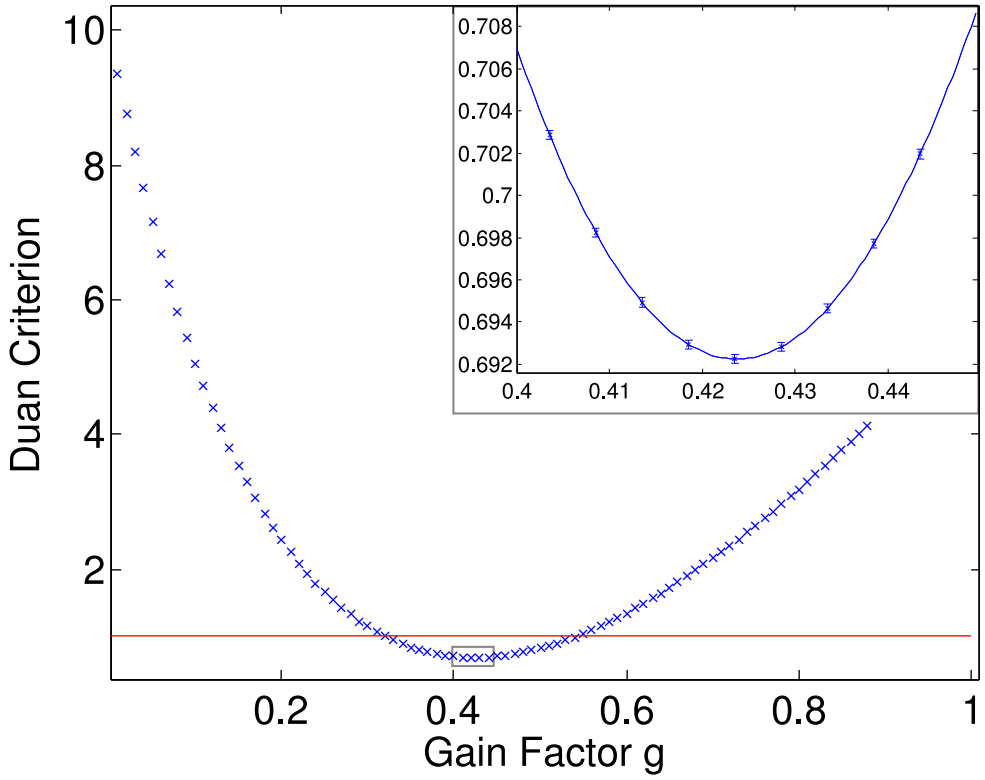

FIG. 2: **Graph proving the recovered entanglement of the two mode state $\hat{\rho}_{A'B'}$.** The experimental values for the Duan criterion are depicted in dependence of the gain factor g. Due to the attenuation of the mode B by 50 %, a gain factor about 0.5 yields a value smaller than 1, i.e. below the limit for entanglement (red line). The best entanglement value of 0.6922 ± 0.0002 is shown for $g_{\text{opt}} = 0.4235 \pm 0.0005$. The inset zooms into the interesting section around the minimum. The depicted estimated errors are so small because of the large amount of data taken.

That proves the emergence of entanglement (Fig: 2). The used gain factor g considers the slightly different detector response and the intentional loss of 50 % at Bob's beam splitter. The best entanglement value of 0.6922 ± 0.0002 is shown for $g_{\text{opt}} = 0.4235 \pm 0.0005$. This is the only step of the protocol, where entanglement emerges, thus demonstrating the remarkable possibility to entangle the remote parties Alice and Bob by sending solely a separable auxiliary mode C'.

Discussion

Role of dissipation. The performance of the protocol can be explained using the structure of the displacements (1). These displacements effectively render a coupling to the environment so that quantum correlations of a particular structure are shared with the environment and redistributed within the global system allowing to recover entanglement between the distant modes A' and B' in the final step. That is, after imposing the correlated displacements, the three modes are not in a product state any more. This can be interpreted as dissipation to a common reservoir, which can even lead to the creation of entanglement as shown in [28, 29].

Role of discord. All non-product separable Gaussian states have non-zero Gaussian discord, that is, exhibit quantum correlations, which are beyond entanglement [30]. In our scheme, from the resource state prepared by David and through the protocol, the state of the modes held by Alice and Bob has non-zero discord which grows with increasing magnitude of displacements. It is in perfect agreement with the recent findings that for entanglement distribution by separable states to work, discord between modes A and B should be initially present. The entanglement gain is bound by the discord across the partition $A'B|C'$ after A and C have interacted [16, 17]. Note that this latter requirement is directly related to the particular properties of our global state after the interaction of modes A and C on Alice's beam splitter described in the introductory part. That is, the possibility to distribute entanglement by a separable ancilla can be attributed to the fact, that the state $\hat{\rho}_{ABC}$ prepared by David is a separable quantum state possessing discordant correlations. Furthermore, the state $\hat{\rho}_{A'BC'}$ contains discord and entanglement across $A'|BC'$ splitting and is separable and discordant across $C'|A'B$ splitting as required by the protocol.

Role of classical information. Entanglement distribution without sending entanglement also highlights vividly the important role played by classical information in quantum information protocols. Classical information lies in our knowledge about all the correlated displacement involved. This allows the communicating parties (or David on their behalf) to adjust the displacements locally to recover through clever noise addition quantum resources initially present in the input quantum squeezed states. Mode C' transmitted from Alice to Bob carries on top of the sub-shot noise quadrature of the input squeezed state the displacement noise which is anticorrelated with the displacement noise of Bob's mode. Therefore,

when the modes are interfered on Bob's beam splitter, this noise partially cancels out in the output mode B' when the light quadratures of both modes add. Moreover, the residual noise in Bob's position (momentum) quadrature is correlated (anticorrelated) with the displacement noise in Alice's position (momentum) quadrature in mode A', again initially squeezed. Due to this the total variance of two modes A' and B' drops below the value for separable states and thus entanglement between Alice's and Bob's modes emerges. The difference between the two protocol versions lies merely in the way how classical information is used. In the original protocol, the classical information is retained by David and he is responsible for clever tailoring of correlated noise. Bob evokes the required noise cancellation by carrying out the final part of global operation via superimposing his mode with the ancilla on BS_{BC}. In the experimentally implemented protocol, David shares part of his information with Bob, giving Bob a possibility to activate entanglement a posteriori, by using his part of classical information after the quantum operation is carried out (see Fig. 1). Thus entanglement distribution in our case is truly performed via a dual classical and quantum channel, via classical information exchange in combination with the transmission of separable quantum states.

Methods

State Preparation The two identically squeezed modes A and C required by the protocol are implemented as two polarization squeezed modes [26, 31–33]. Each of these modes is generated by launching two orthogonally polarized femtosecond pulses ($\sim$200 fs) with balanced powers onto the two birefringent axes of a polarization maintaining fiber (FS-PM-7811, Thorlabs, 13 m). The pump source is a soliton-laser emitting light at a center wavelength of 1559 nm and a repetition rate of 80 MHz. By exploiting the optical Kerr effect of the fibers, the orthogonally polarized pulses are individually quadrature squeezed and subsequently temporally overlapped with a relative phase of $\pi/2$, resulting in a circular polarized light beam. The relative phase is actively controlled using an interferometric birefringence compensator including a piezoelectric transducer (PZT) and a locking loop based on a 0.1 % tap-off signal after the fiber.

The modulation of each polarization squeezed mode in the dark-plane is implemented using electro-optical modulators (EOM). By applying a sinusoidal voltage V_{mod}, the bire-

fringence of the EOMs changes at a frequency of 18.2 MHz. We adjust the half-wave plates in front of the EOMs such that the modulation occurs along the direction of the squeezed observable. An additional quarter-waveplate is necessary to compensate for the residual birefringence of the EOM, even if no modulation voltage is applied.

Finally, the two identically prepared modes A and C are interfered on a balanced beam splitter (BS_{AC}) with a fixed relative phase of $\pi/2$ by controlling the optical path length of one mode with a PZT and a locking loop. This results in equal intensities of both output modes.

Measurement Process To study the correlations between mode A' and B', multiple pairs of Stokes observables $(\hat{S}_{A',\theta}, \hat{S}_{B',\theta})$ are measured. In particular, the covariance matrix $\gamma_{A'B'}$ is determined by measuring five pairs of observables: $(\hat{S}_{A',0^\circ}, \hat{S}_{B',0^\circ})$, $(\hat{S}_{A',90^\circ}, \hat{S}_{B',0^\circ})$, $(\hat{S}_{A',0^\circ}, \hat{S}_{B',90^\circ})$, $(\hat{S}_{A',90^\circ}, \hat{S}_{B',90^\circ})$ and $(\hat{S}_{A',45^\circ}, \hat{S}_{B',45^\circ})$. Here, θ is the angle in the $\hat{S}_1$-$\hat{S}_2$-plane between $\hat{S}_{0^\circ}$ and $\hat{S}_\theta$. The same procedure can be applied for the determination of $\gamma_{A'C'}$. The uncertainties indicated for the measured matrices have been determined by dividing the data set into 10 distinct parts and calculating the covariance matrices for the individual parts. The standard deviation of the elements of the covariance matrices gives the estimated statistical error.

For the measurements of the different Stokes observables, we use two Stokes measurement setups, each comprising a rotatable half-wave plate, a Wollaston prism and two balanced detectors. The difference signal of one pair of detectors gives one Stokes observable $\hat{S}_\theta$ in the $\hat{S}_1$-$\hat{S}_2$-plane, depending on the orientation of the half-wave plate.

The signals are electrically down-mixed using an electric local oscillator at 18.2 MHz, which is in phase with the modulation used in the state preparation step. With this detection scheme, the modulation translates to a displacement of the states in $\hat{S}_1$-$\hat{S}_2$-plane. The difference signal is low pass filtered (1.9 MHz), amplified and then digitized using an analog-to-digital converter card (GaGe Compuscope 1610) at a sampling rate of 10M samples/s. After the measurement process we digitally low pass filter the data by an average filter with a window of 10 samples.

Due to the ergodicity of the problem, we are able to create a Gaussian mixed state computationally from the data acquired as described above. By applying 80 different modulation depths V_{mod} to each of the EOMs we acquire a set of 6400 different modes. From these set of modes we take various amounts of samples, weighted by a two dimensional

Gaussian distribution (see also Fig. 4). The post-processing for the recovery of the entanglement is performed on the measured raw data of mode B'. Therefore, the displacement of the individual modes caused by the two modulators is calibrated. By means of this calibration, suitable displacements are applied digitally. The classical noise inherent in the mode B' is completely removed. A part of the classical noise associated with $\hat{S}_{A',0^\circ}$ is subtracted from $\hat{S}_{B',0^\circ}$, while the same fraction of the noise in $\hat{S}_{A',90^\circ}$ is added to $\hat{S}_{B',90^\circ}$. In this way, the noise partially cancels out in the calculation of Duan's criterion and allows to reveal the entanglement. We chose the fraction as in (1), which is compatible with the separability of the transmitted mode C' from the subsystem $(A'B)$ in the scenario with modulation on mode B before the beam splitter BS_{BC}.

Acknowledgements

L. M. acknowledges project P205/12/0694 of GAČR. N. K. is grateful for the support provided by the A. von Humboldt Foundation. The project was supported within the framework of the BMBF grant "QuORep". We thank Christoffer Wittmann and Christian Gabriel for fruitful discussions.

Author contributions

All authors contributed substantially to this work.

Competing financial interests

The authors declare no competing financial interests.

Note

Recently, an experiment has been presented in [34], which is based on a similar protocol. The main difference consists in the fact that it starts with entanglement which is hidden and recovered with thermal states. For this implementation no knowledge about classical information has to be communicated to Bob, besides the used thermal state. By contrast the setup presented in this work exhibits entanglement only at the last step of the protocol. Thus both works give good insights on different aspects of the theoretically proposed protocol [19]. Another independent demonstration of a similar protocol based on discrete variables was recently presented in [35].

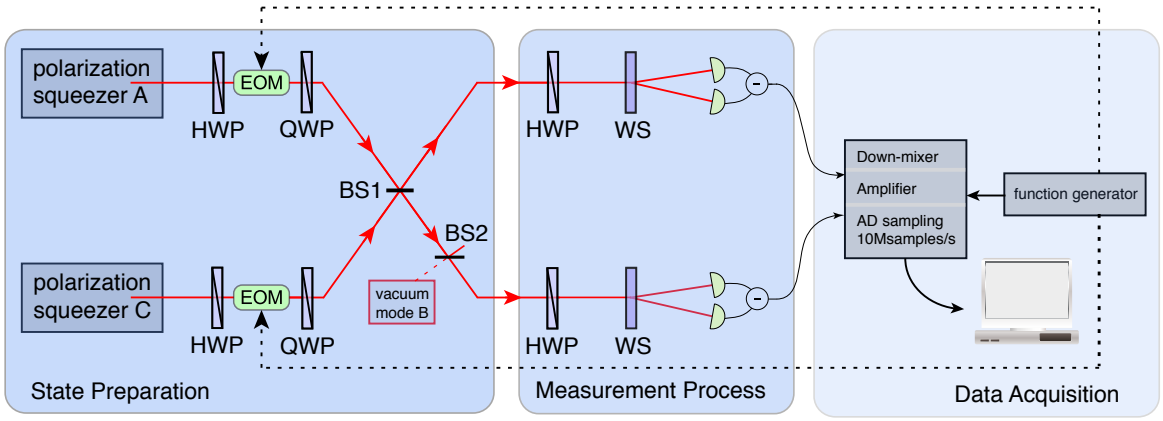

FIG. 3: **Sketch of the experimental setup** Used abbreviations: HWP: Half-wave plate; QWP: Quarter-wave plate; EOM: Electro-optical modulator; BS1/BS2: Beam splitter; WS: Wollaston prism; (State Preparation) The polarization of two polarization squeezed states (A and C) is modulated using EOMs and sinusoidal voltages (18.2 MHz) from a function generator (dotted lines). The HWPs before the EOMs are used to adjust the direction of modulation to the squeezed Stokes variable, whereas the QWPs compensate for the stationary birefringence of the EOMs. The such prepared modes interfere with a relative phase of $\pi/2$ on a balanced beam splitter (BS1). In the last step of the protocol, the mode C' interferes with the vacuum mode B on a second balanced beam splitter (BS2). (Measurement Process) A rotatable HWP, followed by a WS and a pair of detectors from which the difference signal is taken allows to measure all possible Stokes observables in the $\hat{S}_1$-$\hat{S}_2$-plane. To determine the two-mode covariance matrix $\gamma_{A'B'}$ all necessary combinations of Stokes observables are measured. Removing the second beam splitter of the state preparation allows us to measure the covariance matrix of the two-mode state ($A'C'$). (Data Acquisition) To achieve displacements of the modes in the $\hat{S}_1$-$\hat{S}_2$-plane we electronically mix the Stokes signals with a phase matched electrical local oscillator (18.2 MHz). The resulting signals are low pass filtered (1.9 MHz) and amplified before they are sampled by an analog-to-digital converter with a sampling rate of 10 M samples/s. The first step of the digital post processing made on the computer is an average filter with a window of 10 samples to further low pass filter the signals. After that the Gaussian mixed state is prepared.

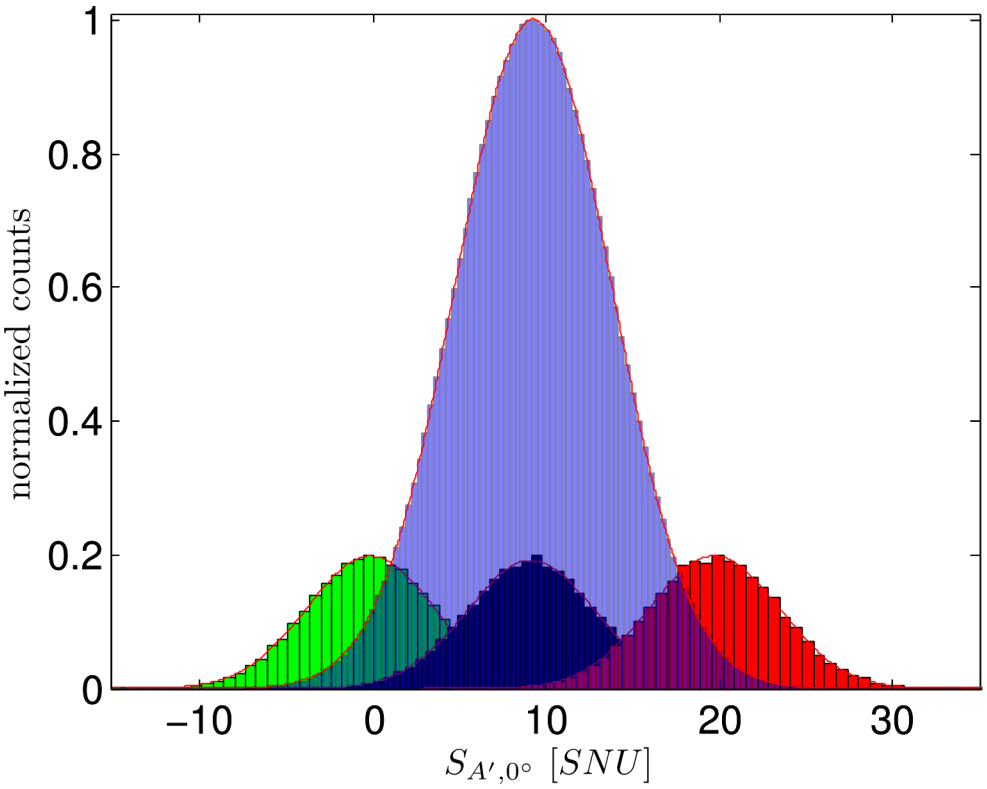

FIG. 4: **Histogram plots for $\hat{S}_{A',0^\circ}$ of the Gaussian mixed state (blue) and three exemplary individual modes.** The transparent blue histogram depicts the Gaussian distribution of the mixed state, it is normalized to its maximum value. The red curve is a Gaussian fit to the histogram. The other three plots show the distributions for three out of 6400 displaced individual modes, the mixed state is composed of. They visualize the fact that the displacement of the individual modes does not affect the shape of their distribution. Gaussian functions have been fitted to them (red curves). The normalization is chosen such that they can be depicted in the same plot as the histogram of the mixed state.

Appendix A: Gaussian states

We implement the entanglement distribution protocol using optical modes which are systems in infinitely-dimensional Hilbert state space. An N-mode system can be conveniently characterized by the quadrature operators $\hat{x}_j, \hat{p}_k$, $j,k = 1,2,\ldots,N$ satisfying the canonical commutation rules $[\hat{x}_j, \hat{p}_k] = i\delta_{jk}$ which can be expressed in the compact form as

$$[\hat{\xi}_j, \hat{\xi}_k] = \mathrm{i}\Omega_{jk}. \tag{A1}$$

Here we have introduced the vector of quadratures $\hat{\xi} = (\hat{x}_1, \hat{p}_1, \ldots, \hat{x}_N, \hat{p}_N)$ and

$$\Omega_N = \bigoplus_{i=1}^{N} J, \quad J = \begin{pmatrix} 0 & 1 \\ -1 & 0 \end{pmatrix}, \tag{A2}$$

is the symplectic matrix.

The present protocol relies on Gaussian quantum states. As any standard Gaussian distribution, a Gaussian state $\hat{\rho}$ is fully characterized by the vector of its first moments

$$d = \mathrm{Tr}\left(\hat{\rho}\hat{\xi}\right), \tag{A3}$$

and by the covariance matrix γ with elements

$$\gamma_{jk} = \mathrm{Tr}[\hat{\rho}\{\hat{\xi}_j - d_j\mathbb{1}, \hat{\xi}_k - d_k\mathbb{1}\}], \tag{A4}$$

where $\{\hat{A}, \hat{B}\} = \hat{A}\hat{B} + \hat{B}\hat{A}$ is the anticommutator. A real symmetric positive definite matrix describes a covariance matrix of a physical quantum state if and only if it satisfies the condition [36]:

$$\gamma + \mathrm{i}\Omega \geq 0. \tag{A5}$$

The separability of Gaussian states can be tested using the positive partial transpose (PPT) criterion. A single mode j is separable from the remaining $N-1$ modes if and only if the Gaussian state $\hat{\rho}$ has a positive partial transposition $\hat{\rho}^{T_j}$ with respect to the mode j [24, 37]. On the level of the covariance matrices, the partial transposition is represented by a matrix $\Lambda_j = \left(\bigoplus_{i\neq j=1}^{N-1} \mathbb{1}_i\right) \oplus \sigma_z^{(j)}$, where $\sigma_z^{(j)} = \mathrm{diag}(1,-1)$ is the diagonal Pauli z-matrix of mode j. The matrix $\gamma^{(T_j)}$ corresponding to a partially transposed state $\hat{\rho}^{T_j}$ reads $\gamma^{(T_j)} = \Lambda_j \gamma \Lambda_j^T$. In terms of the covariance matrix, one can then express the PPT criterion in the following form. A mode j is separable from the remaining modes if and only if [24, 37]

$$\gamma^{(T_j)} + \mathrm{i}\Omega \geq 0. \tag{A6}$$

The PPT criterion (A6) is a sufficient condition for separability only under the assumption of Gaussianity of all the states involved. In our experiment, however, non-Gaussian states can be generated for which this criterion represents only a necessary condition. Therefore it can fail in detecting entanglement.

Appendix B: Analysis of non-Gaussianity

There are two sources of imperfections in our experimental set up that are potential sources of non-Gaussianity. These are phase fluctuations and the modulation of the initial squeezed states before the first beam splitter. They are discussed in the following sections.

1. Phase fluctuations

The experiment includes an interference of the modes A and C on a beam splitter, which is the first beam splitter BS_{AC} in the protocol. Imperfect phase locking at this beam splitter might cause a phase drift resulting in a non-Gaussian character of the state $\hat{\rho}_{A'C'}$ after the beam splitter. The phase fluctuations can be modelled by a random phase shift of mode A before the beam splitter described by a Gaussian distribution $P(\phi)$ with zero mean and variance σ^2. Denoting the operator corresponding to a beam splitter transformation as $\hat{\mathcal{U}}$ and the phase shift ϕ on mode A as $\hat{V}_A(\phi)$, the state $\hat{\rho}_{A'C'}$ can be linked to the state $\hat{\rho}_{AC}$ before the onset of phase fluctuations as

$$\hat{\rho}_{A'C'} = \int_{-\infty}^{\infty} P(\phi)\hat{\mathcal{U}}\hat{V}_A(\phi)\hat{\rho}_{AC}\hat{V}_A^{\dagger}(\phi)\hat{\mathcal{U}}^{\dagger}d\phi. \tag{B1}$$

Hence we can express the measured covariance matrix $\gamma_{A'C'}$ given in Eq.(2) of the main letter, and the vector of the first moments d' of the state $\hat{\rho}_{A'C'}$ in terms of the covariance matrix γ_{AC} and the vector of the first moments d of the input state $\hat{\rho}_{AC}$. For this it is convenient to define matrices D and D' of the first moments with elements $D_{ij} = d_i d_j$ and $D'_{ij} = d'_i d'_j$, $i, j = 1, \ldots, 4$. Using Eq. (B1) and after some algebra, one gets the transformation rule for the matrix of the first moments in the form $D' = U\Sigma D\Sigma U^T$, where U describes the beam splitter on the level of covariance matrices. $\Sigma = \mathrm{diag}(e^{-\frac{\sigma^2}{2}}, e^{-\frac{\sigma^2}{2}}, 1, 1)$ is a diagonal matrix. Similarly we get the covariance matrix

$$\gamma_{A'C'} = U\left(\Sigma\gamma_{AC}\Sigma + \pi \oplus 0\right)U^T, \tag{B2}$$

where 0 is the 2×2 zero matrix and

$$\pi = \frac{(1 - e^{-\sigma^2})^2}{2}(A + \alpha) + \frac{1 - e^{-2\sigma^2}}{2} J(A + \alpha)J^T. \tag{B3}$$

Here the matrix A is the 2×2 matrix with elements $A_{ij} = (\gamma_{AC})_{ij}$, $i, j = 1, 2$, α is the 2×2 matrix with elements $\alpha_{ij} = 2D_{ij}$, $i, j = 1, 2$, and J is defined in Eq.(A2). Similar to Ref. [34] we can now invert the relation (B2) and express the input covariance matrix γ_{AC} via the output covariance matrix $\gamma_{A'C'}$ and the first moments after the beam splitter BS_{AC} as

$$\gamma_{AC} = \Sigma^{-1} U^T \gamma_{A'C'} U \Sigma^{-1} + \tilde{\pi} \oplus 0, \tag{B4}$$

where

$$\tilde{\pi} = \frac{(1 - e^{\sigma^2})^2}{2}(\tilde{A} + \tilde{\alpha}) + \frac{1 - e^{2\sigma^2}}{2} J(\tilde{A} + \tilde{\alpha})J^T. \tag{B5}$$

The 2×2 matrices $\tilde{A}$ and $\tilde{\alpha}$ possess the elements $\tilde{A}_{ij} = (U^T \gamma_{A'C'} U)_{ij}$ and $\tilde{\alpha}_{ij} = 2(U^T D' U)_{ij}$, $i, j = 1, 2$.

Our estimate for the variance of the phase fluctuations is $\sigma^2 = 0.02^\circ$ and the vector d' of the measured mean values of the state $\hat{\rho}_{A'C'}$ reads

$$d' = (-0.208, 9.876, 13.32, 1.78). \tag{B6}$$

By substituting these experimental values for σ^2 and d' in Eq. (B4) and using the beam splitter with the measured transmissivity $T = 0.49$ we get a legitimate covariance matrix γ_{AC} before the phase fluctuations as can be easily verified by checking the condition (A5).

Provided that the state with the covariance matrix γ_{AC} is classical it can be expressed as a convex mixture of products of coherent states. Gaussian distributed phase fluctuations and a beam splitter preserve the structure of the state, hence the state after the first beam splitter cannot be entangled. The covariance matrix γ_{AC} determines a physical Gaussian quantum state. Moreover, the covariance matrix possesses all eigenvalues greater than one and therefore the state is not squeezed [36] which is in a full agreement with the fact that modulations of modes A and C completely destroy the squeezing. It then follows that this Gaussian state is classical and it therefore transforms to a separable state after the first beam splitter.

Inversion (B4) thus allows us to associate a Gaussian state before the phase fluctuations with the covariance matrix $\gamma_{A'C'}$ measured after the first beam splitter. The separability properties of the state after the beam splitter can then be determined from the non-classicality properties of this Gaussian state.

2. Gaussianity of the utilized states

We have paid great attention on the modulations on modes A and C to preserve Gaussian character of the state $\hat{\rho}_{A'C'}$. Our success can be visually inspected at the examples in Fig. 4 of the main letter, which illustrates that both the modulation and the subsequent Gaussian mixing faithfully samples the required Gaussian shape.

Besides this raw visual check we have also tested quantitatively Gaussianity of the involved states by measuring higher-order moments of the Stokes measurements on modes A' and C'. Specifically, we have focused on the determination of the shape measures called skewness S and kurtosis K defined for a random variable x as the following third and fourth standardized moments

$$S = \frac{\mu_3}{s^3}, \quad K = \frac{\mu_4}{s^4}, \tag{B7}$$

where $\mu_k = \langle (x - \langle x \rangle)^k \rangle$ is the kth central moment, $\langle x \rangle$ is the mean value and $s = \sqrt{\mu_2}$ is the standard deviation.

Skewness characterizes the orientation and the amount of skew of a given distribution and therefore informs us about its asymmetry in the horizontal direction. Gaussian distributions possess skewness of zero. The exemplary values of skewness for various measurement settings are summarized in the Table I.

TABLE I: Skewness S for Stokes measurements on modes A' and C' in different measurement directions.

Measurement	$S_{A',0^\circ}$	$S_{A',90^\circ}$	$S_{C',0^\circ}$	$S_{C',90^\circ}$
Skewness$\times 10^3$	6.240 ± 0.781	-1.478 ± 0.563	10.123 ± 0.727	1.106 ± 0.830

The skewness can vanish also for the other symmetrical distributions, which may, however, differ from a Gaussian distribution in the peak profile and the weight of tails. These

differences can be captured by the kurtosis which is equal to 3 for Gaussian distributions. The exemplary values of kurtosis for various measurement settings are summarized in the Table II.

TABLE II: Kurtosis K for Stokes measurements on modes A' and C' in different measurement directions.

Measurement	$S_{A',0^\circ}$	$S_{A',90^\circ}$	$S_{C',0^\circ}$	$S_{C',90^\circ}$
Kurtosis	$2.971 \pm 2.211 \times 10^{-3}$	$2.986 \pm 1.852 \times 10^{-3}$	$2.972 \pm 1.978 \times 10^{-3}$	$2.992 \pm 1.568 \times 10^{-3}$

The tables reveal that the measured probability distributions satisfy within the experimental error the necessary Gaussianity conditions $S = 0$ and $K = 3$. More sophisticated normality tests can be performed, which is beyond the scope of the present manuscript.

[1] Schrödinger, E. Die gegenwärtige situation in der quantenmechanik. *Naturwiss.* **23**, 807–812 (1935).

[2] Einstein, A., Podolsky, B. & Rosen, N. Can quantum-mechanical description of physical reality be considered complete? *Phys. Rev.* **47**, 777–780 (1935).

[3] Reid, M. D. Demonstration of the Einstein-Podolsky-Rosen paradox using nondegenerate parametric amplification. *Phys. Rev. A* **40**, 913–923 (1989).

[4] Wiseman, H. M., Jones, S. J. & Doherty, A. C. Steering, entanglement, nonlocality, and Einstein-Podolsky-Rosen paradox. *Phys. Rev. Lett.* **98**, 140402 (2007).

[5] Bell, J. S. On the Einstein-Podolsky-Rosen paradox. *Physica* **1**, 196-200 (1964).

[6] Cerf, N. J. & Adami, C. Negative entropy and information in quantum mechanics. *Phys. Rev. Lett.* **79**, 5194–5197 (1997).

[7] Horodecki, M., Oppenheim, J. & Winter A. Partial quantum information. *Nature* **436**, 673–676 (2005).

[8] Bennett, C. H., Brassard, G., Crépeau, C., Jozsa, R., Peres, A. & Wotters, W. K. Teleporting an unknown quantum state via dual classical Einstein-Podolsky-Rosen channels. *Phys. Rev. Lett.* **70**, 1895–1899 (1993).

[9] Žukowski, M., Zeilinger, A., Horne, M. A. & Ekert, A. K. "Event-ready-detectors" Bell experiment via entanglement swapping. *Phys. Rev. Lett.* **71**, 4287–4290 (1993).

[10] Briegel, H.-J., Dür, W., Cirac, J. I. & Zoller, P. Quantum repeaters: The role of imperfect local operations in quantum communication. *Phys. Rev. Lett.* **81**, 5932–5935 (1998).

[11] Ekert, A. K. Quantum cryptography based on Bell's theorem. *Phys. Rev. Lett.* **67**, 661–663 (1991).

[12] Bennett, C. H. & Wiesner, S. J. Communication via one- and two-particle operators on Einstein-Podolsky-Rosen states. *Phys. Rev. Lett.* **69**, 2881–2884 (1992).

[13] Raussendorf, R. & Briegel, H. J. A one-way quantum computer. *Phys. Rev. Lett.* **86**, 5188–5191 (2001).

[14] Pan, J.-W., Bouwmeester, D., Weinfurther, H. & Zeilinger, A. Experimental entanglement swapping: Entangling photons that never interacted. *Phys. Rev. Lett.* **80**, 3891–3894 (1998).

[15] Cubitt, T. S., Verstraete, F. & Cirac, J. I. Separable states can be used to distribute entanglement. *Phys. Rev. Lett.* **91**, 037902 (2003).

[16] Streltsov, A., Kampermann, H. & Bruß, D. Quantum cost for sending entanglement. *Phys. Rev. Lett.* **108**, 250501 (2012).

[17] Chuan, T. K., Maillard, J., Modi, K., Paterek, T., Paternostro, M. & Piani, M. Quantum discord bounds the amount of distributed entanglement. *Phys. Rev. Lett.* **109**, 070501 (2012).

[18] Kay, A. Using separable Bell-diagonal states to distribute entanglement. *Phys. Rev. Lett.* **109**, 080503 (2012).

[19] Mišta, L. Jr. & Korolkova, N. Improving continuous-variable entanglement distribution by separable states. *Phys. Rev. A* **80**, 032310 (2009).

[20] Dür, W. & Cirac, J. I. Activating bound entanglement in multiparticle systems. *Phys. Rev. A* **62**, 022302 (2000).

[21] Mišta, L. Jr. & Korolkova, N. Gaussian multipartite bound information. *Phys. Rev. A* **86**, 040305 (2012).

[22] Peres, A. Separability criterion for density matrices. *Phys. Rev. Lett.* **77**, 1413–1415 (1996).

[23] Horodecki, M., Horodecki, P. & Horodecki, R. Separability of mixed states: necessary and sufficient conditions. *Phys. Rev. A* **223**, 1-8 (1996).

[24] Werner, R. F. & Wolf, M. M. Bound entangled Gaussian states. *Phys. Rev. Lett.* **86**, 3658–3661 (2001).

[25] Duan, L.-M., Giedke, G., Cirac, J. I. & Zoller, P. Inseparability criterion for continuous variable systems. *Phys. Rev. Lett.* **84**, 2722 (2000).

[26] Heersink, J., Josse, V., Leuchs, G. & Andersen, U. L. Efficient polarization squeezing in optical fibers *Opt. Lett.* **30** (10), 1192 – 1194 (2005).

[27] Korolkova, N., Leuchs, G., Loudon, R., Ralph, T. C. & Silberhorn, C. Polarization squeezing and continuous-variable polarization entanglement *Phys. Rev. A* **65**, 052306 (2002).

[28] Benatti, F. & Floreanini, R. Entangling oscillators through environment noise. *J. Phys. A: Math. Gen.* **39**, 2689 (2006).

[29] Korolkova, N. Influence of modal loss on the quantum state generation via cross-Kerr nonlinearity. *Phys. Rev. A* **79**, 053832 (2009).

[30] Adesso, G. & Datta, A. Quantum versus classical correlations in Gaussian states. *Phys. Rev. Lett.* **105**, 030501 (2010).

[31] Leuchs, G., Ralph, T. C., Silberhorn, C. & Korolkova, N. Scheme for the generation of entangled solitons for quantum communication. *J. Mod.Opt.* **46**, 1927-1939 (1999).

[32] Silberhorn, C., Lam, P. K., Weiß, O., König, F., Korolkova, N. & Leuchs, G. Generation of continuous variable Einstein-Podolsky-Rosen entanglement via the Kerr nonlinearity in an optical fiber *Phys. Rev. Lett.* **86** 4267–4270 (2001).

[33] Dong, R, Heersink, J., Yoshikawa, J.-I.,Glöckl, O., Andersen, U. L. & Leuchs, G. An efficient source of continuous variable polarization entanglement. *New J. Phys.* **9**, 410 (2007).

[34] Vollmer, C. E., Schulze, D., Eberle, T., Händchen, V., Fiurasek, J. & Schnabel, R. Experimental entanglement distribution by separable states *arXiv:1303.1082* (2013).

[35] Fedrizzi, A., Zuppardo, M., Gillett, G. G., Broome, M. A., de Almeida, M., Paternostro, M., White, A. G. & Paterek, T. Experimental distribution of entanglement via separable states *arXiv:1303.4634* (2013).

[36] Simon, R., Mukunda, N. & Dutta, B. Quantum-noise matrix for multimode systems: U(n) invariance, squeezing, and normal forms. *Phys. Rev. A* **94**, 1567–1583 (1994).

[37] Simon, R. Peres-Horodecki Separability criterion for continuous variable systems. *Phys. Rev. Lett.* **84**, 2726–2729 (2000).